



Characterisation of PZT thin film micro-actuators using a silicon micro-force sensor

Fabrice F.C. Duval^{a,*}, Stephen A. Wilson^a, Graham Ensell^b, Nicolas M.P. Evanno^c, Markys G. Cain^d, Roger W. Whatmore^{a,1}

^a School of Industrial and Manufacturing Science, Cranfield University, Bedfordshire MK43 0AL, UK

^b INNOS Limited, Mountbatten Building, Highfield, Southampton, Hampshire SO17 1BJ, UK

^c Rolls-Royce Plc, Strategic Research Centre, Sina-28, P.O. Box 31, Derby DE24 8BJ, UK

^d National Physical Laboratory, Hampton Road, Teddington, Middlesex TW11 0LW, UK

Received 12 October 2005; received in revised form 20 March 2006; accepted 29 March 2006

Abstract

This paper reports on the measurements of displacement and blocking force of piezoelectric micro-cantilevers. The free displacement was studied using a surface profiler and a laser vibrometer. The experimental data were compared with an analytical model which showed that the PZT thin film has a Young's modulus of 110 GPa and a piezoelectric coefficient $d_{31,f}$ of 30 pC/N. The blocking force was investigated by means of a micro-machined silicon force sensor based on the silicon piezoresistive effect. The generated force was detected by measuring a change in voltage within a piezoresistors bridge. The sensor was calibrated using a commercial nano-indenter as a force and displacement standard. Application of the method showed that a 700 μm long micro-cantilever showed a maximum displacement of 800 nm and a blocking force of 0.1 mN at an actuation voltage of 5 V, within experimental error of the theoretical predictions based on the known piezoelectric and elastic properties of the PZT film.

© 2006 Elsevier B.V. All rights reserved.

Keywords: PZT; Cantilevers; Vibrometry; Force sensors; Blocking force

1. Introduction

Piezoelectric micro-electro-mechanical systems (MEMS) have been studied in many areas related to precision position control [1], acoustic [2], pressure and gas sensors [3]. Lead zirconate titanate (PZT) ceramics have been extensively used due to their superior piezoelectric properties [4] for a wide range of sensors and actuators. For instance, micro-actuators have been fabricated using a combination of sol-gel derived PZT and surface micro-machining techniques [5,6]. The power output is directly proportional to the thickness of the piezoelectric film, so thicker films are of great importance. The direct use of bulk PZT ceramics for MEMS devices is not trivial since it

requires expensive and laborious processing to achieve thicknesses below 100 μm . The sol-gel technique [7] is a feasible way to deposit PZT films for MEMS with thicknesses from 1 to 10 μm . The method offers good control of the PZT stoichiometry and is inexpensive. Nevertheless it is limited in the thickness of single layers that can be grown due to crack occurrence as a result of thermal expansion mismatch between PZT and silicon substrate [8].

It is well known that thin film properties are significantly lower than the bulk figures and that films' properties largely depend on processing conditions. Knowledge of these properties is of great importance for the modelling of new device designs. Full experimental characterisation is also needed because modelling cannot always take all the parameters into account, such as stress gradients, physical imperfections. Intensive research has been carried out to investigate the properties of piezoelectric cantilever beams. Due to the small thickness of the beams, the displacement lies in the \AA – μm range. Non-contact techniques such as interferometry [9], atomic force microscopy (AFM) [10], fibre optic sensor (FOS) [11], laser scanning vibrometer

* Correspondence to: Institut d'Electronique, de Microelectronique et de Nanotechnologies, Cite Scientifique, Avenue Poincare, BP 6, 59652 Villeneuve d'Ascq, France.

E-mail address: fa_duval@yahoo.fr (F.F.C. Duval).

¹ Present address: Tyndall National Institute, Lee Maltings, Prospect Row, Cork, Ireland.

(LSV) [12] have been successfully used. The latter is particularly suitable to characterise the dynamic displacement because it measures the velocity of the beam based on the Doppler shift effect. Another main characteristic of these devices to investigate is the blocking force, which is not readily achievable using the previously mentioned techniques. It is common practice to estimate the blocking force knowing the moment of inertia, I and the maximum displacement (Eq. (1)) [13].

$$F = \frac{3EI\delta}{l^3} = \frac{Ewt^3\delta}{4l^3} \quad \text{Expression of the blocking force} \quad (1)$$

where F is the blocking force, E the Young's modulus, l , w and t , respectively, the length, width and thickness of the beam and δ is the displacement. This, however, does not give a true representation of the blocking force as already shown on macro-scale piezoelectric actuators [14]. To the best of our knowledge nothing has been yet reported on the full load versus displacement characterisation of the blocking force of micro-scale PZT cantilever beams. This paper presents the fabrication of a micro-force sensor that was fabricated and calibrated and then used to measure the blocking force of piezoelectric micro-actuators.

2. The micro-force sensor

2.1. Principle of force measurement

The force sensor is a silicon beam which includes four piezoresistors arranged in a Wheatstone bridge, as shown in Fig. 1: it is a quarter bridge meaning that only one resistor is active, i.e. that on the beam. The active resistor was positioned as close as possible to the fixed end of the beam, where maximum stress occurs. In order to measure the force developed by the actuator to be tested, the latter is to be deflected against the silicon sensor, as shown in Fig. 2.

This change in resistance is related to the force produced by the actuator through calibration curves. Finally, the use of a series of sensors with increasing stiffnesses (i.e. with different thicknesses) allows the full load versus displacement curve (Fig. 3) for the test actuator to be constructed.

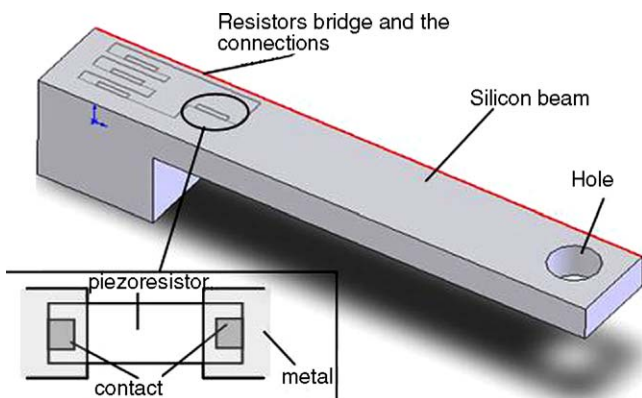


Fig. 1. Schematic of the silicon sensor showing the four resistors and the hole for alignment purpose.

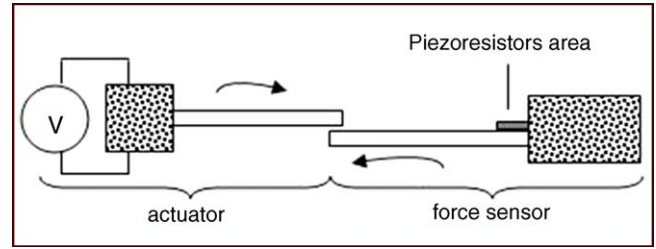


Fig. 2. Schematic of the interaction between actuator and force sensor.

2.2. Piezoresistors design

The p-type piezoresistors were fabricated by ion implanting the silicon surface to obtain maximum control and hence reproducibility between wafers. The piezoresistive coefficient and hence, the sensitivity is governed by the dopant concentration, the orientation of the resistor along the silicon crystallographic axis and the temperature. The sensitivity is expressed as the change in resistance as shown by Eq. (2) [15].

$$\frac{\Delta R}{R} = \pi_L \sigma_L + \pi_T \sigma_T \quad \text{Change in resistance in a piezoresistor} \quad (2)$$

where R and ΔR are the resistance of the piezoresistor and the change in resistance, respectively, σ_L and σ_T the local stresses occurring in the longitudinal and transversal directions, respectively, and π_L and π_T are the longitudinal and transversal piezoresistive coefficients, respectively. Using finite element analysis (FEA) (Intellisuite[®]), it has been found that under specified loading conditions the non-linear influence of transverse loading on the piezoresistors can be neglected. Eq. (2) becomes $\frac{\Delta R}{R} = \pi_L \sigma_L$ with π_L equal to $72E10^{-11} \text{ Pa}^{-1}$ [15] for silicon p-type resistors.

The piezoresistors were designed to be longer than wide to maximise the effect of longitudinal stress. The length has to be small to maximise the amount of tension generated in the resistors. Fig. 4 shows the results of an Intellisuite[®] simulation conducted on a $50 \mu\text{m}$ long piezoresistor (represented as rectangles in Fig. 4) to evaluate how the stress varies when changing the position of the piezoresistor with respect to the fixed end of the beam. The variation in stress along the length is more pronounced. At a distance of $100 \mu\text{m}$ from the edge, the stress is only 70% of the maximum stress. The variation in stress along the width is only less than 1%.

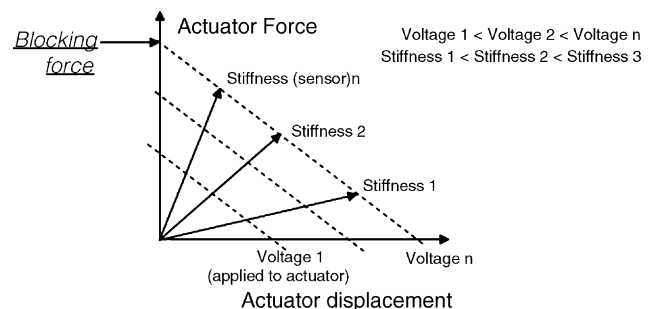


Fig. 3. Schematic of the full load vs. displacement graph.

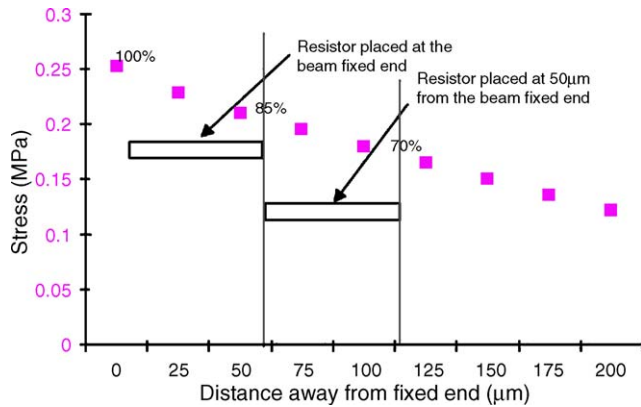


Fig. 4. FEA simulations: stress profile for a $400 \mu\text{m} \times 300 \mu\text{m} \times 100 \mu\text{m}$ ($l \times w \times t$) cantilever when loaded with 0.3 mN as a function of the distance away from the fixed end.

As imposed by the resolution of photolithography and silicon deep reactive ion etching (DRIE), the piezoresistor cannot be placed right at the edge of the cantilever. Fig. 4 also shows that the decrease in stress is less significant if positioning the resistor $50 \mu\text{m}$ away from the fixed end.

The Johnson noise (J_n) or thermal noise, as shown by Eq. (3), is the thermal agitation of electrons in a resistor, which gives rise to a random fluctuation in the voltage across its terminals.

$$J_n = (4k_t TRB)^{1/2} \quad \text{Expression of Johnson noise} \quad (3)$$

where k_t is the Boltzmann constant ($1.38\text{E}-23 \text{ J K}^{-1}$), T the temperature, R the resistance and B is the bandwidth. Using a resistance of $200 \text{ k}\Omega$, a temperature of $25 \text{ }^\circ\text{C}$, the Johnson noise can be estimated at $0.2 \mu\text{V}$ for a 10 Hz bandwidth. It is not anticipated to be a significant factor for the measurement of the piezoresistive voltage because the latter is at least 10 orders of magnitude bigger than the Johnson noise estimated above.

2.3. Micro-force sensor design

This part of the design is concerned with the geometrical dimensions of the force sensors. The width of the cantilevers was fixed at $300 \mu\text{m}$. The dimensions of the cantilevers were calculated using Eqs. (1) and (4).

$$\sigma_{\max} = \frac{6Fl}{wt^2} \quad \text{Maximum stress in a cantilever as a function of the load applied} \quad (4)$$

where σ_{\max} is the maximum stress and F is the force applied to the cantilever.

Table 1
Force sensors properties

Piezoresistor dimensions (μm)			Resistance	Output current (based on a voltage of 10 V)	Cantilever dimensions (μm)			Change in voltage (mV)
l	w	t			l	w	t	
60	10	1	$\sim 200 \text{ k}\Omega$	$\sim 0.04 \text{ mA}$	1000–2600	300	50–200	Few tens of microvolts up to few hundreds of millivolts

Silicon cantilevers were designed to measure blocking forces over the range 0.1 mN up to several hundreds of millinewtons. Calculations were carried out with the view of maximising the maximum stress in the beam (i.e. making the cantilevers as short and thick as possible) because the sensitivity is directly proportional to the stress value (Eq. (2)). The least stiff silicon beam is $2600 \mu\text{m} \times 300 \mu\text{m} \times 50 \mu\text{m}$ and the stiffest is $750 \mu\text{m} \times 300 \mu\text{m} \times 200 \mu\text{m}$ in order to cover the range of force to be investigated. The range of sensors to be made as well as their expected properties are summarised in Table 1. The change in piezoresistive voltage can be expressed for a quarter-bridge by Eq. (5).

$$\Delta V = \frac{1}{4} \frac{\Delta R}{R} V_0 \quad \text{Change in piezoresistive voltage} \quad (5)$$

where ΔV is the change in voltage and V_0 is the input voltage of 10 V .

It is vital to ensure that the minimum forces (μN range) can generate enough stress to cause a detectable change in voltage. The minimum force expected to be measured is $100 \mu\text{N}$, which corresponds to an expected stress of about 2 MPa for a $50 \mu\text{m}$ thick and $2600 \mu\text{m}$ long force sensor that would generate a change in voltage of 4 mV . Fig. 5 presents the change in stress and voltage when applying the minimum range of forces onto the stiffest sensors (i.e. $200 \mu\text{m}$). The minimum change in voltage to be expected is about $50 \mu\text{V}$ (Fig. 5) which is reasonably well above the level of noise calculated above.

3. Experimental

3.1. Micro-force sensors fabrication

The 5 masks process used was based on surface and bulk micro-machining techniques. Devices were made from double-sided polished 100 mm (1 0 0) silicon on insulator (SOI) wafers, n-type ($10\text{--}20 \Omega \text{ cm}$) with a handle layer thickness of $400 \mu\text{m}$ and three device layers of 50 , 100 and $200 \mu\text{m}$. A 600 nm thick silicon oxide layer is grown by wet oxidation at $1000 \text{ }^\circ\text{C}$. Piezoresistor windows are opened using mask 1 and the oxide is etched by reactive ion etching (RIE) in a mixture of CHF_3 and Ar gases. Another thinner layer of silicon oxide is grown at $950 \text{ }^\circ\text{C}$ in oxygen. This 40 nm thick layer helps to prevent ion implantation damage at the silicon surface during subsequent activation anneals. Boron is implanted with a dose of $4 \times 10^{11} \text{ cm}^{-2}$ at 70 keV and activated at $1000 \text{ }^\circ\text{C}$ for 30 min in nitrogen. Following this, contact windows (Fig. 6) are implanted with $5 \times 10^{15} \text{ cm}^{-2} \text{ BF}_2$ at 70 keV using mask 2.

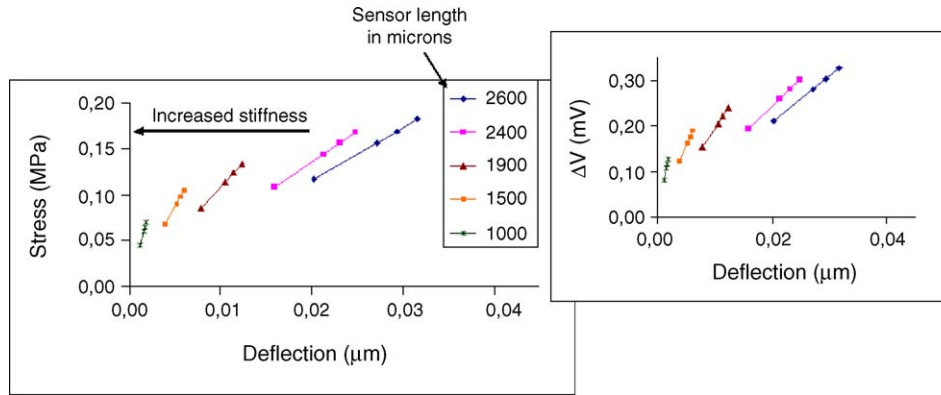


Fig. 5. Modelling: (a) stress vs. deflection and (b) ΔV vs. deflection for sensors (thickness = 200 μm) with forces varying from 0.1 to 0.15 mN.

The 40 nm thick oxide is etched by RIE, and the junctions are activated at 1100 °C for 10 s by rapid thermal annealing. The Al/Si metal is then deposited by sputtering in argon and etched in a gas mixture of chlorine and silicon tetrachloride using mask 3. After patterning, the metal is alloyed in H_2/N_2 for 30 min at 450 °C. The next steps are to release the cantilever structures. First the 600 nm thick oxide is etched using a Plasmatech 80 RIE using mask 4. The silicon device layer is also etched down to the buried oxide (BOX) layer using mask 4 by DRIE, and a second deep etch is conducted from the back of the wafer, using mask 5, to release the structures. Finally the BOX is wet-etched in a solution of 10 vol.% HF for 45 min. Fig. 7 shows a scanning electron microscope (SEM) picture of a micro-force sensor: the four piezoresistors as well as the metal connections and the hole can be observed.

3.2. Piezoelectric cantilevers fabrication

A three masks process was developed to fabricate the piezoelectric micro-actuators. The process flow can be found in Fig. 8. The fabrication starts with a 100 mm single-sided polished bare (1 0 0) silicon wafer. A layer of sol-gel zirconium oxide (ZrO_2) is first deposited. The procedure can be found elsewhere [16]. This layer helps to grow crack-free PZT on silicon as Imura [17] showed that PZT cracked when directly deposited on to silicon. The bottom electrode (Ti 8 nm/Pt 100 nm) is deposited using a multi-target radio frequency (RF) magnetron sputtering system (Nordiko Limited). A thin layer of titanium is first sputtered to act as an adhesion promoter between ZrO_2 and platinum. The next step is the PZT deposition. This is carried out by depositing 30 layers of a 0.4 M 52/48 PZT solution by spin coating the solution at 3000 rpm for 30 s. The sol synthesis is reported else-

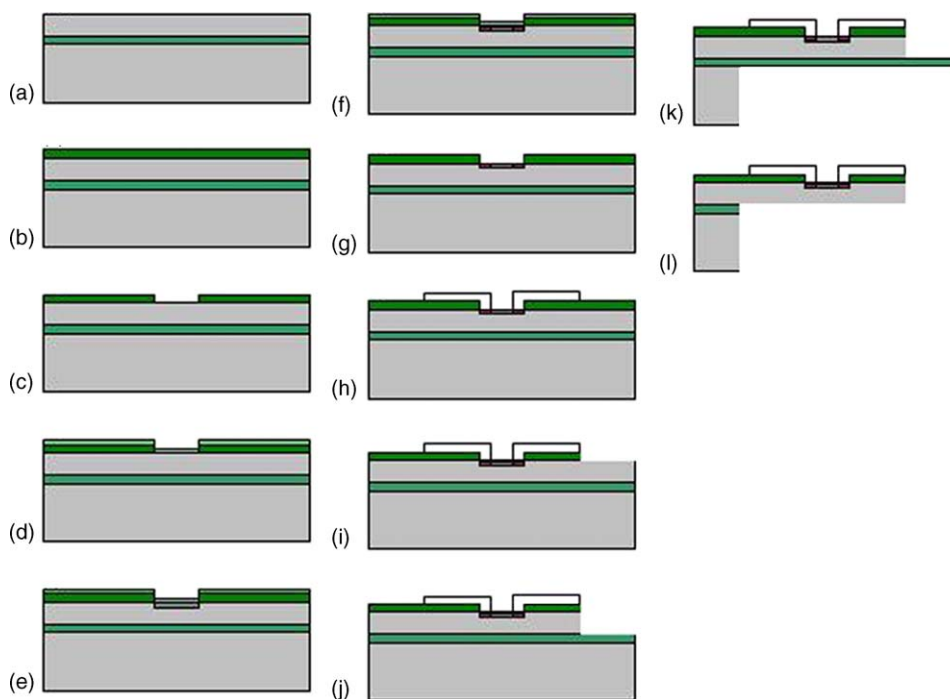


Fig. 6. Piezoresistive sensor flowchart, (a) SOI wafer ($\text{Si}/\text{SiO}_2/\text{Si}$), (b) 600 nm oxide, (c) oxide etch (mask 1), (d) 40 nm oxide, (e) first implantation, (f) second implantation (mask 2), (g) 40 nm oxide etch, (h) metal sputtering (mask 3), (i) 600 nm oxide etch (mask 4), (j) front silicon deep etch (mask 4), (k) back silicon deep etch (mask 5) and (l) BOX wet etch.

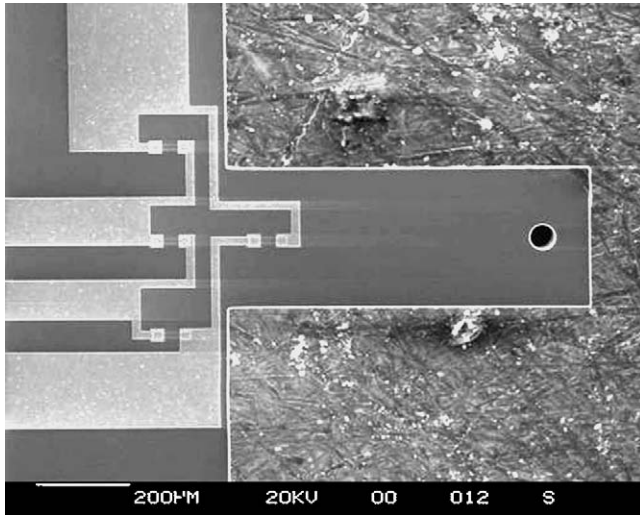


Fig. 7. SEM photomicrograph of the micro-force sensor.

where [18]. Each layer, approximately 100 nm thick, is baked at 200 °C for 30 s and crystallised at 600 °C for 5 min for the first 10 layers and 3 min from the 11th layer onwards. X-ray diffraction (XRD) showed the PZT layer to be fully crystallised, with a randomly orientated crystalline structure. Dielectric measurements were made using a Wayne Kerr precision component analyser 6425 at 1 kHz. It showed a dielectric loss of 1.5% and a relative permittivity of 900. The top electrode was obtained by a lift-off technique based on a bi-layered resist coating (LOR-2A and S1818 (Chestech UK)). The PZT was wet-etched in a HF/HCl/H₂O (0.5/4.5/95, v/v/v) solution (I) for 30 s, rinsed in deionised water for 10 s, and put in a nitric acid (30 vol.%) solution (II) for 45 s to dissolve the PbClF precipitate formed with the first solution. This operation is repeated: 30 s in (I) and 3 min in (II). This gave an approximate etch rate of 40 nm/s similar to that described by Baborowski [5]. The bottom electrode and the zirconia layer were etched using a RIE Plasmatech 80 using Ar,

and a mixture of Ar and CHF₃, respectively. The front silicon is deep etched in a STS ICP etcher (DRIE) using a mixture of SF₆, O₂ and C₄F₈ gases. Deep etch was conducted from the back side to release the free-standing structures.

3.3. Calibration measurements

The calibration was carried out using NPL's (National Physical Laboratory, Teddington, UK) nano-mechanical testing machine, NTM3D [19]. The calibration is concerned with applying a defined displacement onto the beam and measuring the corresponding change in piezoresistive voltage and the generated force. This equipment allows simultaneous measurement of forces and displacements in three orthogonal directions, and has enough free space to mount a wide range of fixtures in a well controlled environment. The NTM3D is built on two distinct parts functioning along the same principle allowing the out-of-plane (*z*-axis) control through the vertical stage, and the in-plane (*x* and *y* axes) control through the horizontal stage. Four capacitance sensors with sub-nanometre resolution, from Queensgate Instruments, are incorporated in the stages. The first two provide force and displacement measurement along the *z*-axis, while the remaining two provide horizontal force measurement in the *x* and *y* directions. Horizontal displacements are imposed through the internal encoding of the inchworm motors, with a minimum displacement of 4 nm. The system is fully enclosed in a vibration isolated cabinet, mounted on a Melles–Griot active optical table. Specimen alignment is carried out optically, through the use of a charge coupled device (CCD) video camera positioned at 30° with the *X–Y* plane. The contact with the force sensor was made using a 30 μm diameter diamond tip.

3.4. Displacement and force measurements

Prior to carrying out any measurements on the PZT cantilevers, one corner of the wafer was etched in a HF/HCl/H₂O (0.5/4.5/95, v/v/v) solution to expose the bottom electrode. The devices were poled by applying a voltage between the top and bottom electrode. The poling was conducted for 10 min at a voltage varying between 20 and 40 V and a temperature of 130 °C. The static displacement under an applied voltage was assessed using a Dektak surface profiler. The stylus was scanned at the tip of the beam across the width while applying a voltage on and off to create a step height in the measurement profile. The step height was taken as the measured displacement. The quasi-static displacement was assessed using a laser scanning vibrometer (LSV-Polytech OFV 3001). An AC voltage (peak to peak) between 0.5 and 10 V was used. The blocking force was finally measured by deflecting the piezoelectric beam against a set of calibrated silicon force sensors. The force sensor was brought in contact with the test actuator under an optical microscope. The use of high precision {*X*, *Y*, *Z*} positioning stages (Physics Instruments PM-500 and PM-400) enabled to accurately position the force sensor with the actuator, with respect to the hole created at the end of the sensor beam. The contact between the two beams was also accurately done using the *Z* stage with a 100 nm increment. The PZT cantilever was actuated DC caus-

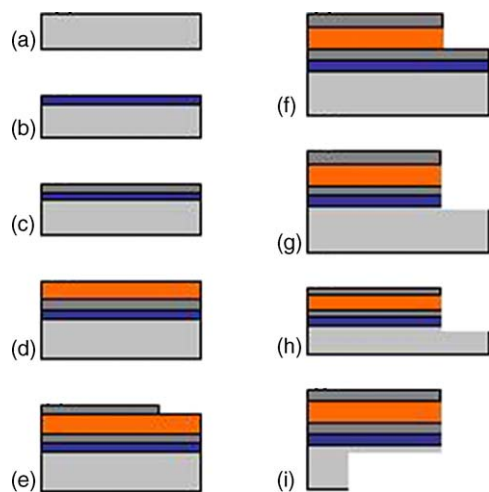


Fig. 8. Piezoelectric cantilever flowchart (a) Si wafer, (b) ZrO₂, (c) Ti/Pt, (d) PZT, (e) Ti/Pt (mask 1), (f) PZT wet etch (mask 2), (g) Ti/Pt and ZrO₂ dry etch (mask 2), (h) Si DRIE (mask 2) and (i) Si DRIE (mask 3).

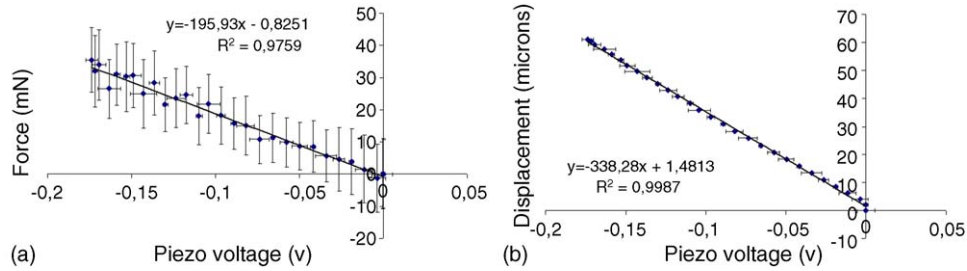


Fig. 9. Calibration curves: (a) force vs. voltage, (b) displacement vs. voltage for a 2600 μm long and 100 μm thick force sensor.

ing the silicon beam to deflect and a change in voltage through the bridge. The latter was used to obtain force and displacement by referring to the calibration curves formed as described above.

4. Force sensors calibration

Prior to calibration, the sheet resistance was measured: uniform figures with a variation of 5% were found between chips on the same wafer. The piezoresistive behaviour of the sensors was also studied by recording I – V (current–voltage) curves, between 9 and 10 V, showing ohmic behaviour. The same bridge (i.e. same position on wafer) was tested for each thickness at two opposite points of the Wheatstone bridge. Each force sensor was separately calibrated.

A typical pair of calibration curves, as recorded by the NTM3D for a 2600 μm long and 100 μm thick force sensor, are presented in Fig. 9, showing force versus piezoresistive voltage in Fig. 9a and displacement versus piezoresistive voltage in Fig. 9b. The sensitivity of the force sensor for the force and displacement is given by the slope of the calibration curves. The sensitivity is the change in displacement or force applied to the force sensor that is required to produce a unit change in piezoresistive voltage. Table 2 summarises the slope coefficients obtained on several different beams. It shows that the force slope increases and the displacement slope decreases as the beam thickness increases, as expected.

A Young's modulus of silicon of about 120–130 GPa was required to obtain a good fit with the force versus displacement curves. The silicon Young's modulus was checked by measuring beams' resonant frequencies (Eq. (6), [20]) using the LSV.

$$f_r = 0.162 \frac{t}{l^2} \sqrt{\frac{E}{\rho}} \quad \text{Resonant frequency of a cantilever beam} \quad (6)$$

where ρ is the density of the material, i.e. 2330 kg/m^3 for silicon [15]. The devices were mechanically excited using a PZT disc

driven at 1 V AC. Using the measured data, and the equation relating the resonant frequencies to the mechanical properties, the silicon Young's modulus was found to be 132, 118 and 118 GPa for the 50, 100 and 200 μm thickness wafer, respectively. Since the analytical expression of the resonant frequency is truly valid for high ratio length/thickness, the experimental value of 132 GPa matches that used in the model. This value is in excellent agreement with the literature value for (1 0 0) silicon [21]. Knowing the Si Young's modulus, the experimental data (displacement and force versus change in piezoresistive voltage) were fitted using Eqs. (1) and (5) by adjusting the piezoresistive coefficient. The latter was found to vary between 18 and $44 \times 10^{-11} \text{ Pa}^{-1}$. These values are lower than the maximum theoretical value of $72 \times 10^{-11} \text{ Pa}^{-1}$ and the smallest value were obtained for the 50 μm thick wafers. Discrepancies between wafers were expected because it was found from the I – V curves that the wafers had quite different I – V characteristics.

5. Piezoelectric actuators

5.1. Free displacement measurements of the actuators

The displacement was investigated using the LSV system as well as a contact method, a Dektak surface profiler. The surface profiler gives the static displacement at DC voltages and the LSV a quasi-static displacement, taken at a frequency much lower than the first resonant frequency. The latter was obtained using the LSV by applying a burst chirp signal to excite the device over a wide range of frequencies, i.e. between 10 Hz and 200 kHz. The resonant frequency was recorded for different cantilever lengths as shown in Fig. 10. The fit is better for longer beams: this was expected since the analytical equation for the resonant frequency is only valid for high ratio length/thickness.

The experimental curve (Fig. 10) was compared with the analytical expression for the resonant frequency of a cantilever beam, as shown in Eq. (7) [22], to extract the PZT thin film Young's modulus. The actuator is considered as being a bi-

Table 2
Force and displacement slopes and piezoresistive coefficient for several force sensors

Thickness (μm)	Length (μm)	Piezoresistive coefficient (10^{-11} Pa^{-1})	Force sensitivity (mN/V)	Displacement sensitivity ($\mu\text{m}/\text{V}$)
50	2600	18	107	1598
100	2600	42	196	327
200	2600	44	773	160

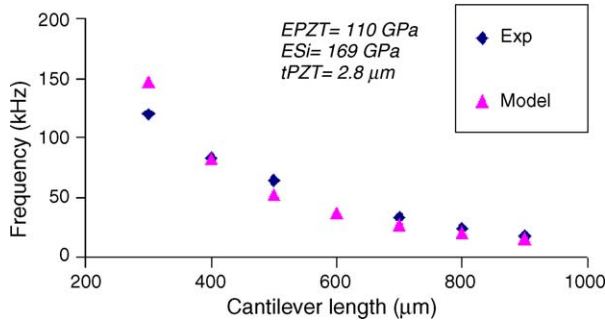


Fig. 10. Resonant frequency as a function of the cantilever length.

layered cantilever made of silicon and PZT. The other materials (electrodes and zirconium oxide) were not taken into account as their thickness is not significant.

$$f_r = \frac{3.52t}{4\pi L^2} \sqrt{\frac{E_p}{3\rho_p} \left[\frac{A^2 B^2 + 2A(2B + 3B^2 + 2B^3 + 1)}{(1 + BC)(AB + 1)(1 + B)^2} \right]^{1/2}}$$

Resonant frequency of a unimorph beam (7)

where f_r is the resonant frequency of the beam, L the beam length, t the beam thickness (silicon + PZT), E_p the PZT Young's modulus, ρ_p the PZT density, A the Young's moduli ratio of silicon and PZT, B being the thickness ratio of silicon and PZT and C is the density ratio of silicon and PZT.

The silicon and PZT thicknesses were determined from SEM examination to be 10 and 2.8 μm , respectively. The (1 0 0) silicon Young's modulus was fixed at 169 GPa [21]. The PZT density was taken as the bulk value (7700 kg/m^3) [23]. The PZT Young's modulus was the varying parameter and a value of 110 GPa, i.e. similar to that reported by Fang et al. [24] for 52/48 PZT films, was used to obtain a good fit with the experimental graph. A micrograph of the PZT cantilever is shown in Fig. 11.

Fig. 12 presents the displacement of a 900 μm long beam recorded using both the surface profiler and the LSV. The displacement measured by the vibrometer is in good agreement with that obtained using the Dektak surface profiler. The latter gives a true static displacement but it is not very precise: this is because the surface of the beam is rough making an uncertainty of 100 nm in the measurements. The effect of the poling voltage on the measured displacement was also studied. An increase from 20 to 30 V did not show a significant increase

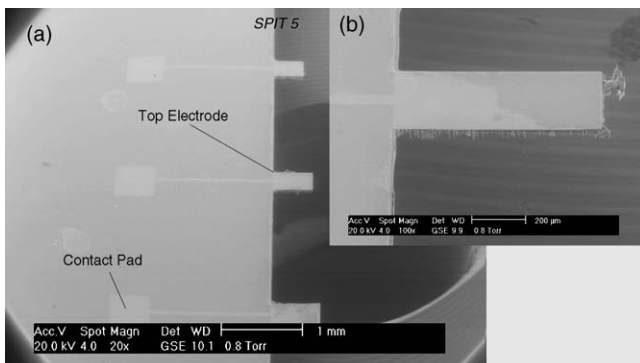


Fig. 11. SEM photomicrographs of a PZT cantilever.

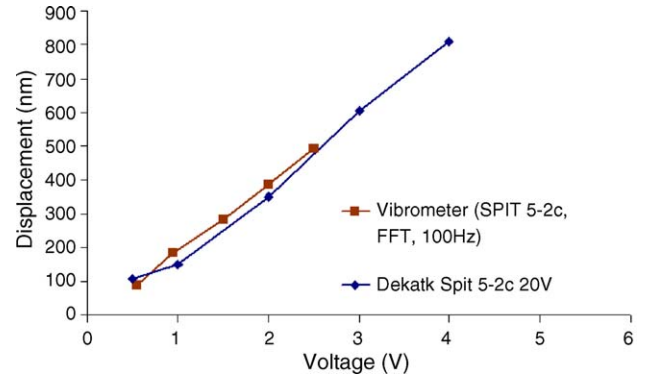


Fig. 12. Displacement (Dektak and vibrometer) of a 900 μm long cantilever beam poled at 20 V.

in displacement. Further increase in the poling voltage up to 40 V (130 kV/cm) led to dielectric breakdown. Hence, 20 V was taken as the optimum voltage and subsequent poling was conducted at this level.

The experimental displacement curves were compared with the analytical model described by Wang and Cross [22] (Eq. (8)).

$$\delta = \frac{3L^2}{2t} \frac{2AB(1 + B)^2}{A^2 B^4 + 2A(2B + 3B^2 + 2B^3) + 1} d_{31} V$$

Displacement of a unimorph actuator (8)

where d_{31} is the piezoelectric coefficient in pC/N and V is the electric field in V/m . The varying parameter was the d_{31} piezoelectric coefficient.

Fig. 13 shows two experimental curves recorded at two different frequencies, 100 and 5000 Hz, for two different beam lengths, 700 and 900 μm . The best fit was obtained using a $d_{31,f}$ of 30 pC/N for both curves. This is only true for the first linear part of the displacement curve for the 900 μm long device. Non-linear characteristics are typical of piezoelectric materials at higher voltages. This value of 30 pC/N is much lower than the bulk value (90 pC/N) [23]. However, reported $d_{31,f}$ values for 52/48 PZT sol–gel films are about 40 pC/N from wafer flexure measurements on sol–gel films [25] and 30 pC/N from piezo-cantilevers coated with (1 1 0) PZT sputtered films [26].

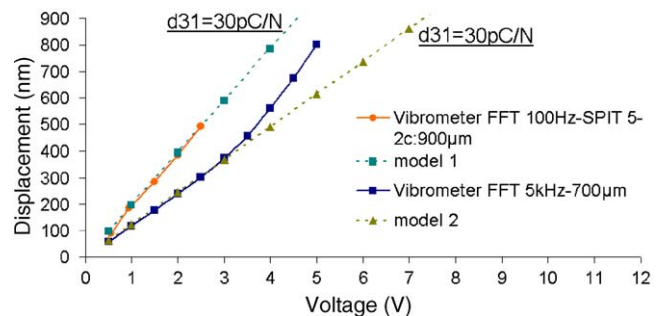


Fig. 13. Experimental (vibrometer) and modelled displacement of a 900 μm cantilever beam.

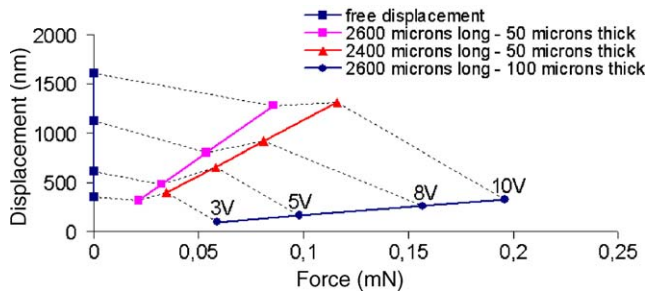


Fig. 14. DC driven micro-actuator (700 μm long) blocking force measurement.

5.2. Force and displacement measurements using the calibrated force sensors

Using the micro-force sensors, the blocking force of the piezoelectric actuators was assessed. The micro-cantilever was set up as described in Fig. 2. The test actuator, positioned above the force sensor, was driven at a voltage between 0 and 10 V DC. The generated change in piezoresistive voltage was recorded using a multimeter. The recorded changes in voltage were used to plot force versus displacement curves by using the calibration curves. The actuator was tested against a series of force sensors with increased stiffness to build the load versus displacement graph as shown in Fig. 14.

The free displacement was measured using the laser vibrometer between 0 and 10 V AC at 5 kHz. Assuming a linear displacement these values were doubled to obtain the displacement between 0 and 10 V DC. The maximum displacement is likely to be greater because the displacement does not follow a linear trend at high electric fields. Three force sensors were tested: two 50 μm thick and one 100 μm thick sensors. The maximum displacement is reduced when the beam is deflected against a force sensor. At the same time the maximum force is increased.

The iso-voltage curves do not exhibit a linear behaviour: this was reported elsewhere for macro-scale actuators [13,14]. The maximum blocking force can be approximated, by linear extrapolation from the stiffest force versus displacement curve, at about 0.25 mN at 10 V and 0.12 mN at 5 V. Assuming a linear behaviour of the iso-voltage curves would lead to a higher value of blocking force (i.e. about 0.4 mN) when taking the maximum free displacement as starting point. The experimental data were compared with the analytical maximum blocking force of a piezoelectric unimorph actuator (Eq. (9)) as described by Wang and Cross [22].

$$F = \frac{3wt^2}{8l} \frac{2AB}{(AB+1)(1+B)} E_P d_{31} V$$

Blocking force of a unimorph actuator (9)

where F is the maximum blocking force. The maximum theoretical blocking force was calculated based on the d_{31} and PZT Young's modulus found from the displacement study, respectively, 30 pC/N and 110 GPa. At 10 V the calculated blocking force is 0.30 mN. This figure is close to the extrapolation from the experimental data.

The experiments show slightly lower values than those predicted by theory. One of the main parameters in the model is the silicon thickness. The latter was approximated from SEM examination and an error of up to 1 μm is possible in this. This would contribute to an uncertainty in the theoretical blocking force of 0.05 mN, which means that the experimental and theoretical values are within experimental error of one another.

6. Conclusion

Piezoelectric micro-cantilevers have been successfully fabricated and characterised. First the static displacement was investigated using two different techniques: profilometry and vibrometry. Both methods gave similar values of displacements. At high voltages it was found that the displacement was not linear. The experimental data were compared with an analytical model which showed a PZT Young's modulus of 110 GPa and a d_{31} piezoelectric coefficient of 30 pC/N.

Secondly the blocking force was studied using micro-force sensors. The latter were first fabricated and calibrated using NPL's nano-mechanical testing machine. The test micro-actuator was deflected against the set of sensors and the generated force and displacement were obtained from the piezoresistive calibration curves. A 700 μm long piezoelectric beam having a PZT thickness of 2.8 μm showed a maximum displacement of 800 nm and a blocking force of 0.1 mN at 5 V. The latter was in relatively good agreement with the value predicted by the analytical model. This work also showed the non-linear nature of blocking force characteristic which has been reported previously. The reasons that an expected linear relationship between force and displacement does not exist are likely to be due to the materials non-linear elastic and piezoelectric properties.

The piezoresistive micro-force sensor, presented here, is a suitable tool to characterise the force/displacement behaviour of micro-devices. Future work aims at testing a large variety of MEMS.

Acknowledgements

This research was carried out as part of the "Measurements for the Processing and Performance of Materials" funded by the UK Department of Trade and Industry. The authors also wish to acknowledge Mr. A. Venturi, Cranfield University, for his expertise and help with making the amplifiers used and Drs. M. Stewart and D. Mendels, National Physical Laboratory, for their help with the use and calibration of the nano-mechanical tester. Funding from the Engineering and Physical Science Research Council under project GR/S45027 is also gratefully acknowledged.

References

- [1] M. Moallem, M.R. Kermani, R.V. Patel, M. Ostojic, Flexure control of a positioning system using piezoelectric transducers, IEEE TCST 2 (5) (2004) 757–762.
- [2] H. Mohamed, D. Polla, E. Ebbini, S. Zurn, Micromachined piezoelectric ultrasonic imaging transducer, in: 44th IEEE Midwest Symposium on Circuits System, Berkeley, CA, August 24–26, 2001, pp. 95–98.

- [3] N. Ledermann, P. Muralt, J. Baborowski, M. Foster, J.P. Pellaux, Piezoelectric $\text{Pb}(\text{Zr}_x\text{Ti}_{1-x})\text{O}_3$ thin film cantilever and bridge acoustic sensors for miniaturised photoacoustic gas detectors, *J. Micromech. Microeng.* 14 (2004) 1650–1658.
- [4] G.H. Haertling, Ferroelectrics ceramics: history and technology, *J. Am. Ceram. Soc.* 82 (4) (1999) 797–818.
- [5] J. Baborowski, Microfabrication of piezoelectric MEMS, *J. Electroceram.* 12 (2004) 33–51.
- [6] S. Zurn, M. Hsieh, G. Smith, D. Markus, et al., Fabrication and structural characterisation of a resonant frequency PZT microcantilever, *Smart Mater. Struct.* 10 (2001) 252–263.
- [7] R.W. Whatmore, Q. Zhang, Z. Huang, R.A. Dorey, Ferroelectric thin and thick films for microsystems, *Mater. Sci. Semicond. Process.* 5 (2002) 65–76.
- [8] N. Ledermann, P. Muralt, J. Baborowski, S. Gentil, K. Mukati, M. Cantoni, A. Seifert, N. Setter, $(100)\text{-Pb}(\text{Zr}_x\text{Ti}_{1-x})\text{O}_3$ textured piezoelectric thin films for MEMS: integration, deposition and properties, *Sens. Actuators A* 105 (2003) 162–170.
- [9] W.Y. Pand, L.E. Cross, A sensitive double beam laser interferometer for studying high frequency piezoelectric and electrostrictive strains, *Rev. Sci. Instrum.* 60 (8) (1989) 2701–2705.
- [10] K.S. Moon, M. Levy, Y.K. Hong, S. Ghimire, Dynamic displacement measurement of PZT-PT unimorph microactuators using atomic force microscopy, in: 17th Annual Meeting of the American Society for Precision Engineering, St. Louis, Missouri, October, 2002, pp. 26–29.
- [11] S.L. Firebaugh, H.K. Charles Jr., R.L. Edwards, A.C. Keeney, S.F. Wilderson, Low-cost deflection measurement for rapid characterisation of microelectromechanical systems (MEMS), in: 20th IEEE Instrumentation and Measurement Technology Conference IMTC03, vol. 1, May 20–22, 2003, pp. 499–502.
- [12] J.S. Burdess, A.J. Harris, D. Wood, R.J. Pitcher, D. Glennie, A system for the dynamic characterisation of microstructures, *J. Micromech. Syst.* 6 (4) (1997) 322–328.
- [13] W.-H. Chu, M. Mehregany, R.L. Mullen, Analysis of tip deflection and force of a bimetallic cantilever microactuator, *J. Micromech. Microeng.* 3 (1993) 4–7.
- [14] M. Cain, M. Stewart, The measurement of blocking force, NPL report MATC (A) 48, National Physical Laboratory, Hampton Road, Teddington, TW11 0LW United Kingdom, September 2001.
- [15] M. Madou, *Fundamentals of Microfabrication*, CRC Press, 1997.
- [16] F.F.C. Duval, R.A. Dorey, Z. Huang, R. Wright, R.W. Whatmore, Fabrication of high frequency PZT composite thick film membranes resonators, *IEEE TUFFC* 51 (2004) 1255–1261.
- [17] M. Imura, Processing of thin film bulk acoustic resonators, Mater of Philosophy Thesis, Cranfield University, 2001.
- [18] J.M. Marshall, Q. Zhang, Z. Huang, R.W. Whatmore, Orientation control of low temperature deposited sol–gel PZT52/48 films, *Ferroelectrics* 318 (2005) 41–48.
- [19] D.A. Mendels, N.M.P. Evanno, A. Cuenat, Determination of the elastic properties of multi-layered foils by the 4-point micro-bending test, *Philos. Mag.* 85 (16) (2005) 1765–1782.
- [20] H. Jianqiang, Z. Changchun, L. Junhua, H. Yongning, Dependence of the resonance frequency of thermally excited microcantilever resonators on temperature, *Sens. Actuators A* 101 (2002) 37–41.
- [21] T. Yi, C.-J. Kim, Measurement of mechanical properties for MEMS materials, *Meas. Sci. Technol.* 10 (1999) 706–716.
- [22] Q.-M. Wang, L.E. Cross, Performance analysis of piezoelectric cantilever bending actuator, *Ferroelectrics* 215 (1998) 187–213.
- [23] B. Jaffe, W. Cook Jr., H. Jaffe, *Piezoelectric ceramics*, New York, 1971.
- [24] T.-H. Fang, S.-R. Jian, D.-S. Chuu, Nanomechanical properties of lead zirconate titanate thin films by nanoindentation, *J. Phys.: Condens. Matter* 15 (2003) 5253–5259.
- [25] J.F. Shepard, P.J. Moses, S. Trolrier-McKinstry, The wafer flexure technique for the determination of the transverse piezoelectric coefficient (d_{31}) of PZT thin films, *Sens. Actuators A* 71 (1998) 133–138.
- [26] M. Toyama, R. Kubo, E. Takata, K. Tanaka, K. Ohwada, Characterisation of piezoelectric properties of PZT thin films deposited on Si by ECR sputtering, *Sens. Actuators A* 45 (1994) 125–129.

Biographies

Fabrice F.C. Duval graduated with his Master of Science in chemistry in 1999 from the Paul Sabatier University in Toulouse (France). He joined the Nanotechnology Group in Cranfield University, Bedfordshire, UK, in September 2000 to undertake his PhD degree, entitled “PZT Thick Films for High Frequency Transducers”. This project involved a novel sol–gel approach to deposit PZT (lead zirconate titanate) films up to $10\ \mu\text{m}$ thick. This was used to fabricate a prototype for novel ultrasonic applications. Since October 2003, he has been conducting postdoctoral work on piezoelectric MEMS actuators.

Stephen A. Wilson undertook his PhD at Cranfield University conducting original research into electric-field structuring of piezoelectric ceramic–polymer composite materials. This work, completed in 1998, introduced a valuable new method of composite assembly which has been patented world-wide. As senior research fellow in the School of Industrial and Manufacturing Science, he has worked on materials development to optimise the performance of advanced piezoelectric sensor arrays for real-time 3D ultrasonic imaging and on design and development of micro-scale ultrasonic motors and piezoelectric bending actuators for use in micro-air vehicles. Further work on advanced materials processing techniques has led to a new integrated fabrication route for thick film piezoelectric micro-actuators, which uses ultra-precision machining of commercial bulk ferroelectric ceramics in combination with standard micro-fabrication techniques. This work was developed as part of the European Growth Project ‘Aeromems II’. Further work on electric field structuring has led to a new micro-manipulation technique to assemble fine scale piezoelectric fibre arrays and novel composite sandwich panels. His research interests are in materials processing issues for micro-scale devices, piezoelectric micro-actuators and MEMS design.

Graham Ensell graduated with his PhD from the Royal Free Hospital School of Medicine, University of London. He is currently technical manager of Innos and also holds a research position in the Nanoscale Systems Integration Research Group in the School of Electronics and Computer Science, University of Southampton. Since 1982, he has collaborated on a wide range of EPSRC funded projects with research groups throughout the UK. His primary role in these projects has been to develop new silicon based processes and technology required to fabricate devices for these projects. The breadth of the topics covered is large and has included integrated circuits, discrete power devices, high voltage integrated circuits, mechanical sensors, medical and biological sensors, actuators, micro-engineering and materials. He has published about 100 papers on silicon devices and fabrication techniques, and is co-author of a book on MEMS mechanical sensors.

Nicolas M.P. Evanno graduated with his Masters of Science in mechanical engineering, in 2002, from the Ecole Nationale Supérieure de Mécanique et des Microtechniques, in Besançon, France. He joined the Functional Materials Research group at NPL in October 2002. His research work was mainly focused on the determination of the elastic properties of materials at very small scales. His role involved the design of mechanical solutions, the development of the software used to run the equipment, as well as the data formatting algorithms and data analysis software, including noise-reducing filters. This work was used to characterise the elastic properties of multi-layered coatings. He also designed and developed a variety of measurement devices including a custom-built rig used to measure the visco-elastic properties of thin polymer films from the resonant properties of quartz crystals in vacuum as a function of temperature (Quartz Crystal Microbalance project).

Markys G. Cain graduated with his PhD from Warwick University in 1990 and spent the next 2 years in the Materials Department of the University of California, Santa Barbara studying thin film epitaxial science. Subsequent research in ceramic composite materials technology in the UK utilised many of the principles learnt at Santa Barbara in the deployment of new interfacial fibre coatings for advanced high temperature ceramic matrix composites for gas turbine applications. Research with Oxford Instruments led to the development of an SEM based instrumented indentation system and he joined NPL in 1997 to lead the Functional Materials Research group. Research activity includes the development of measurement methods to elucidate materials

behaviour in ferroelectric and piezoelectric ceramics and thin film materials. He has published over 80 papers and 2 patents in the field. He is a member of the Institute of Physics.

Roger W. Whatmore graduated with his PhD from Cambridge University in 1977 and spent nearly 20 years working with the GEC Marconi (formerly Plessey) research laboratories at Caswell in the UK on the development and exploitation of ferroelectric materials in a wide range of electronic devices, particularly sensors and actuators, for which work he was awarded

GEC's Nelson Gold Medal in 1993. In October 1994 he took the Royal Academy of Engineering Chair in Engineering Nanotechnology at Cranfield University, where he leads a group developing the use of ferroelectrics in micro-systems and nano-technology. He has published over 200 papers and 30 patents in the field. He is a fellow of the Royal Academy of Engineering and a fellow of the Institute of Materials, Minerals and Mining who in 2003 awarded him the Griffith Medal for Excellence in Materials Science.